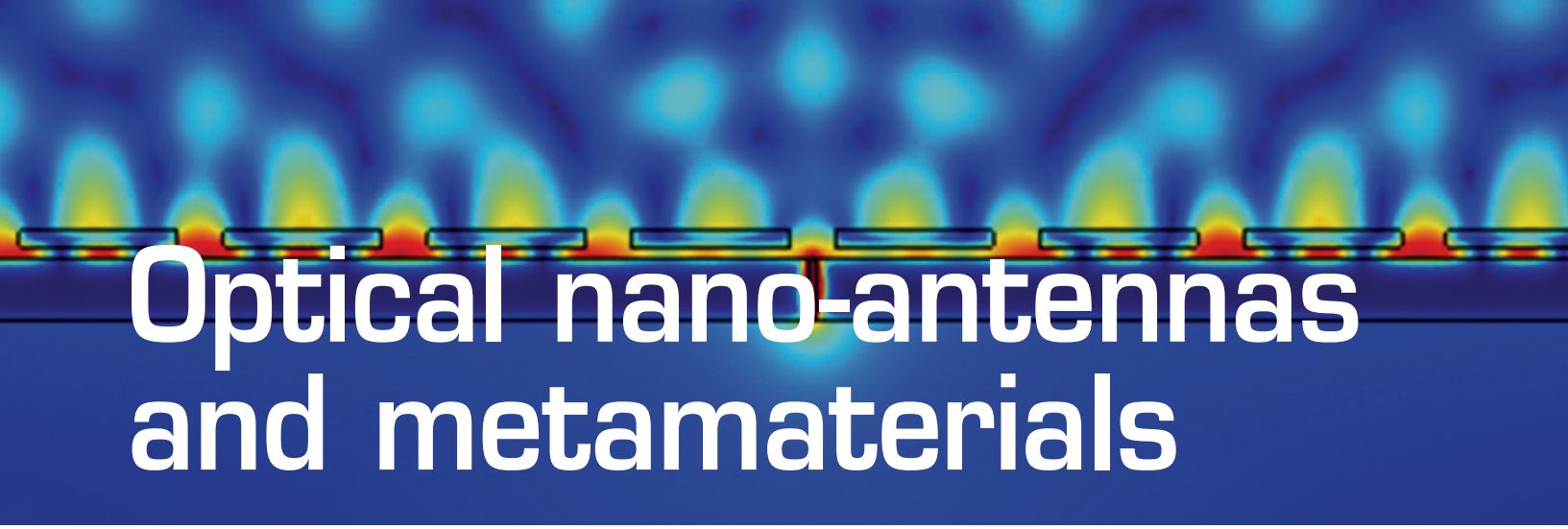

Optical nano-antennas and metamaterials

We review some recent approaches to transmission enhancement and light harvesting based on optical nano-antennas and metamaterials. Nano-cavity antennas are used to enhance the extraordinary transmission of TM-polarized light through vertical nano-slits in a metal film. The enhanced transmission of TE-polarized waves through an array of subwavelength-slits in a thin metal film at low frequencies (including microwave) is also investigated. Light harvesting with a metamaterial cloaking shell is also demonstrated.

Sailing He[1,2,*], Yanxia Cui[1], Yuqian Ye[1], Pu Zhang[1,2], and Yi Jin[1]

[1] Centre for Optical and Electromagnetic Research, State Key Laboratory of Modern Optical Instrumentation, Zhejiang University; JORCEP (Joint Research Centre of Photonics of the Royal Institute of Technology (Sweden) and Zhejiang University), Zijingang Campus, Zhejiang University, China

[2] Division of Electromagnetic Engineering, School of Electrical Engineering, Royal Institute of Technology, S-100 44 Stockholm, Sweden

** E-mail: sailing@kth.se*

Since its discovery[1], extraordinary optical transmission (EOT) through subwavelength apertures including single apertures[2-9] and aperture arrays[10-19] in an opaque metal film have attracted considerable attention. These nanoscale metallic structures possess a wide variety of extraordinary optical properties including beaming[20-22], local filed enhancement[23], and total absorption[24, 25]. Surface plasmons polaritons (SPPs)[26, 27] play an essential role in this phenomenon and have opened up potential applications in lithography[28, 29], biophotonics[30, 31], Raman effect[32], and other areas[33-35]. Besides at visible frequencies, these intriguing phenomena have also been found and investigated at terahertz[36-38], microwave[39-43], acoustic frequencies[44, 45] and matter-waves[46].

Here we review some different approaches to transmission enhancement and light harvesting through nano-apertures, namely, by utilizing optical nano-antennas[9] (note that optical nano-antennas for many other applications have been studied very recently[47-52]) and metamaterials (including slow-light photonic crystal waveguides)[53]. In this article, we will also harvest light with an invisibility metamaterial cloak shell. Metamaterials are composites with subwavelength unit cells dominating some homogenized electromagnetic properties which can not be found in a naturally occurring material[54-56]. Historically, the introduction of this novel concept was initiated decades ago by pursuing the theory of left-handed materials[57, 58]. After the realization of metamaterials at microwave[59] and optical frequencies[60, 61], various predicted effects were demonstrated, such as evanescent wave amplification and subwavelength lensing[62, 63]. We have also studied some potential applications[64-66]. Electromagnetic metamaterials with theoretically arbitrary parameters could be exploited[67]. Similar methods and unit cells have also been developed to investigate single

ISSN:1369 7021 © Elsevier Ltd 2009

negative, or zero-valued effective materials, where electric/magnetic plasmonic and perfect tunneling effects were observed[68, 69]. Using metamaterials, people have studied other promising applications such as perfect absorbers[70], slow light[71], polarization manipulation[72], etc. The method of transformation optics[73] has greatly enlarged the potential application areas of metamaterials, enabling us to design devices according to required characteristics. Invisibility metamaterial cloak is a successful example. The ability to reduce total scattering dramatically has been predicted and verified in various ways, including rigorous analytical solution[74], numerical simulation[75], and proof-of-principle experiment[76, 77]. Various simplified cloak designs[78-80] have been proposed to avoid extreme material parameters. Similar to the widely studied electromagnetic cloaks, cloaks in other fields such as acoustics[81] and matter-waves[82], have also attracted considerable attention.

Enhance transmission of light through metallic nano-slits by utilizing optical nano-antennas

The EOT through a nano-slit in a metal film can be enhanced by introducing nano-antennas. By integration with some optical nano-antennas, the efficiency and spectral response of the EOT or a light-harvesting device could be greatly improved. Recently, Pillai *et al.*[83] put gold nanospheres on the surface of a Si solar cell to increase the spectral response of the thin-film cell. A gold nanorod (GNR) can work as an optical antenna whose resonant frequency can be tuned over a very broad spectrum. A GNR has two surface plasmon resonance (SPR) bands, namely the transverse and longitudinal bands. The longitudinal band is a strong one corresponding to the electron oscillation along the long axis of the nanorod, and can be tuned from visible to near-infrared-red (NIR) region by increasing the aspect ratio (of the width to the length) of the nanorod. In our laboratory we have synthesized GNRs (see[84, 85] and the references therein) according to the classic seed-mediated growth method and the TEM image of our synthesized GNRs is shown in Fig. 1a. GNRs with a SPR peak of 607 nm (corresponding to a GNR with an aspect ratio of 1.8), 650 nm (aspect ratio 2.4) and 710 nm (aspect ratio 2.8) were synthesized and their measured absorption spectra are shown in Fig. 1b (consistent with the results of our numerical simulation). From the photo of the three GNRs (inset in Fig. 1b), one sees that the colors of the three GNR solutions are distinct according to their different SPR resonant bands. We plan to utilize these GNRs to harvest light. Below we show how an appropriately designed plasmonic nanorod (or nano-strip in a 2D case) can be utilized to harvest light and improve the EOT.

First, we present the case of transmission enhancement with a single optical nano-antenna. Fig. 2a shows the two-dimensional (2D) schematic diagram for a metallic rectangular nano-strip (with thickness H_p and width W_p) over a metallic nano-slit of width Ws in a metal film of thickness t (with a distance of d). A plane wave of TM polarization (with the magnetic field perpendicular to the x-z plane) with wavelength λ_0 = 1 μm impinges normally on the top of the structure. Intuitively, the metallic nano-strip over the nano-slit seems to block the incident light. However, through the formation of a resonant nano-cavity antenna, the metallic nano-strip can assist to couple more incident light into the nano-slit and thus enhance the transmission. Both the film and the nano-strip are made of silver, and all the results are calculated with a 2D finite element method (FEM). The transmission efficiency η is defined as the ratio of the integration

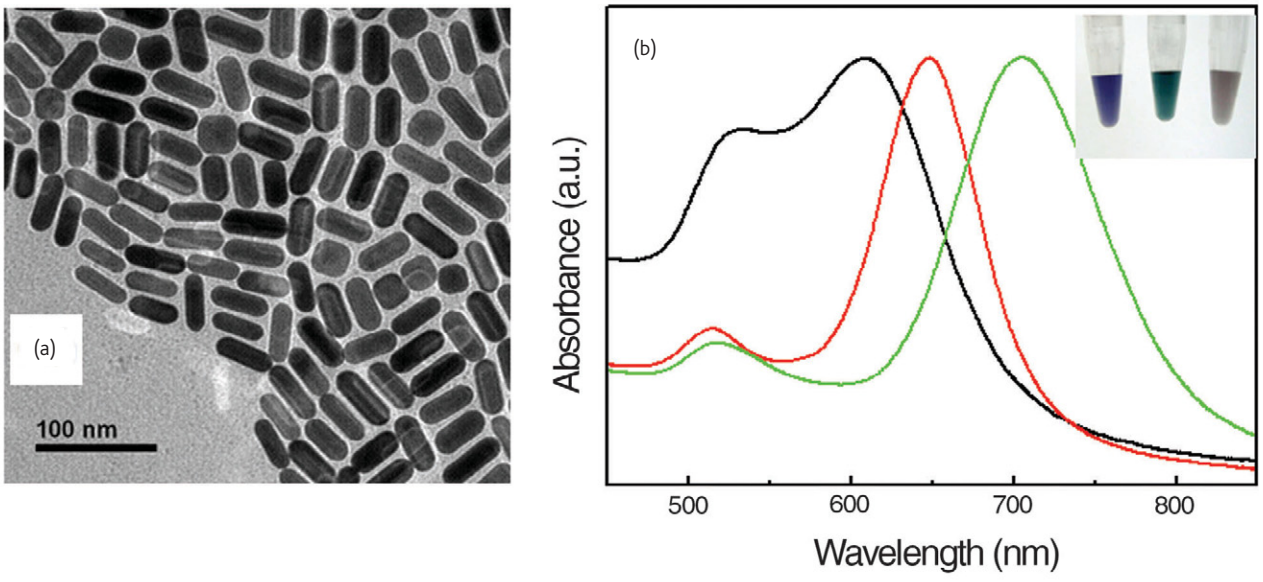

Fig. 1 (a) Measured absorbance spectra of three different types of gold nanorods with SPR peaks at 607 nm, 650 nm, and 710 nm. (b) TEM image of our synthesized gold nanorods with an SPR peak of 650 nm.

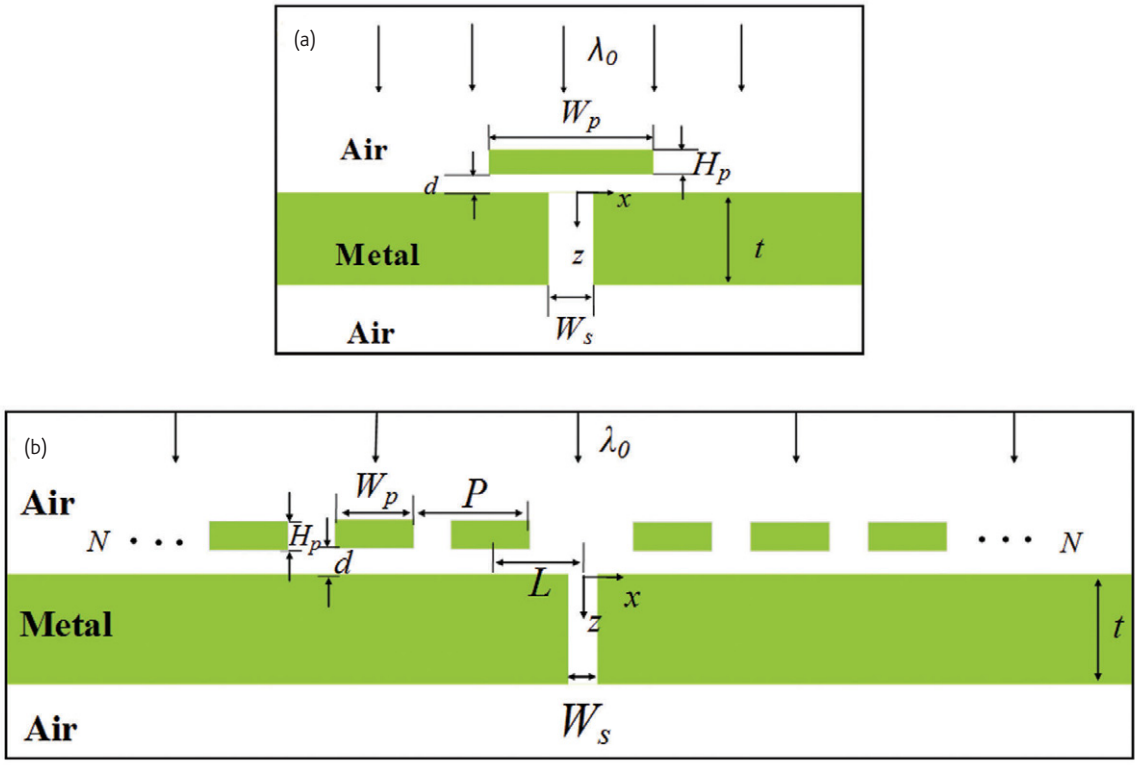

Fig. 2 Configuration of a nano cavity antenna (a) or an array of nano cavity antennas (b) placed a certain distance away from the input surface of a nano-slit aperture milled in a metal film.

of the z-component of the Poynting vector over the output opening (with or without the nano-strip) to that over the input opening of the bare slit (without the nano-strip).

A nano-slit milled in a metallic thin film can form a vertical metal-insulator-metal (MIM) waveguide of finite length, which can give Fabry-Pérot (F-P) resonance in the narrow slit region[3, 5]. The transmission is maximal due to constructive interference for a length phase of even integer of π/2 (related to the effective wavelength in the MIM waveguide) and is minimal for a length phase of odd integer of π/2 (due to destructive interference)[3]. A horizontal MIM waveguide cavity can also be formed by putting a metallic nano-strip over a metal film with an air gap in-between. Fig. 3a shows the distribution of the magnetic field modulus ($|H_y|$) when we put a silver nano-strip (with W_p = 1 μm and H_p = 300 nm) over the silver film (with d = 44 nm) to form constructive interference of three peaks in the horizontal F-P cavity (close to a 3π phase length waveguide). One sees obviously that the metallic nano-strip collects the incident light effectively due to the resonance in the cavity below the nano-strip, and localized field of high

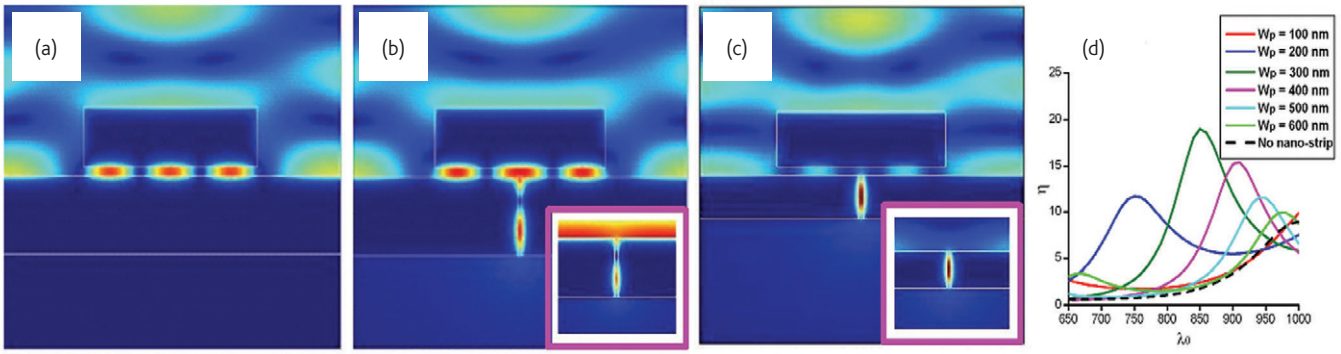

Fig. 3. Distributions of $|H_y|$ for a horizontal resonant MIM cavity (W_p = 1 μm) (a), and a horizontal resonant cavity over a non-resonant nano-slit (b) or a resonant nano-slit (c). The insets in (b) and (c) show the $|H_y|$ distributions for the corresponding cases of a bare nano-slit. (d) Transmission spectrum for various W_p when H_p = 50 nm, d = 44 nm, W_s = 25 nm and t = 240 nm (dashed curve is for the bare nano-slit).

magnitude is accumulated within the horizontal cavity. Then we make a nano-slit in the metal film at a position where the magnetic field in the horizontal resonant cavity is maximal and wish to enhance the extraordinary transmission through the nano-slit in the metal film. The influence of the nano-slit configuration to the field distribution in the horizontal cavity is small (large) when the vertical nano-slit is in a non-resonant (resonant) state. First we consider the case of a non-resonant vertical nano-slit with destructive interference. The inset of Fig. 3b shows the $|H_y|$ distribution for a bare nano-slit with opening width W_s = 25 nm (same in all simulations below) milled in a silver film of 390 nm thickness (as a vertical waveguide of $3\pi/2$ phase length). To see clearly, we plot the field distribution with doubled magnitude in this inset. The transmission efficiency for this bare nano-slit is very low (η = 0.6) and the nano-slit causes little distortion of the field reflected by the silver film. Fig. 3b shows the field distribution when there is a silver nano-strip over this non-resonant nano-slit (opened at the center where the magnetic field is maximal in the horizontal resonant cavity). The resonant cavity antenna over the non-resonant nano-slit brings an enhanced transmission, and the energy flowing out of the nano-slit aperture is enhanced by a factor of 5 as compared with that for the non-resonant bare nano-slit in the inset of Fig. 3b. The inset of Fig. 3c shows the $|H_y|$ distributions for a resonant bare nano-slit with t = 240 nm (corresponding to a vertical MIM waveguide of π phase length). An output transmission efficiency η = 7.8 is achieved, attributed to the constructive interference in the vertical MIM waveguide of finite length. When the silver nano-strip (same as Fig. 3a, b) is put over the resonant nano-slit as shown in Fig. 3c, the horizontal cavity can no longer keep its optimal internal field distribution for harvesting light and the cavity antenna does not work any more. Thus, the energy flowing into the nano-slit is small and η is only 3.6, lower than η in the inset of Fig. 3c. To achieve an efficient receiving antenna for harvesting light (from incident light to SPPs) and further enhancing transmission, the width of the metallic nano-strip should be carefully designed to form a resonant cavity and the height of the nano-strip should also be small enough. When we choose W_p = 1410 nm and H_p = 50 nm, the transmission for the resonant nano-slit can be greatly enhanced to η = 17.5 (124% larger than η = 7.8 for a resonant bare nano-slit). Fig. 3d shows the transmission spectrum for various antenna widths (W_p) when H_p = 50 nm and d = 44 nm. This illustrates the tunability of the optical nano-cavity antenna for harvesting light of desired wavelength. This is quite similar to the tunability of the absorption peak of GNRs for different aspect ratios as shown in Fig. 1b. Some other properties can be found in our recent work[9].

The light transmission enhanced by a single nano-antenna is still not high enough. This can be improved by replacing the single nano-antenna with an array of nano-antennas. Fig. 2b shows the schematic diagram for an array of nano-antennas formed by two metallic rectangular nano-strip arrays (of period P, width W_p, thickness H_p, and number N) on the left and right sides of the vertical nano-slit over a metal film. The distance between the nano-slit center and the nearest nano-strip center (slit-to-strip distance) is denoted by L. Fig. 4 shows the $|H_y|$ distribution after the resonant nano-slit (t = 240 nm) is assisted by a nano-cavity antenna array with P = 900 nm, W_p = 700 nm, L = 450 nm, H_p = 60 nm, d = 50 nm and N = 6. The enhanced transmission through the nano-slit is quite high (η = 128.3), which is 16.4 times of that for the bare resonant nano-slit (η = 7.8) and 6 times larger than that for the single nano-cavity antenna case (η = 17.5). The array of nano-strips could generate some strong surface plasmon wave (SPW) on the input surface. The nano-slit cavity can also generate some reflected SPW near its input opening, whose intensity is much smaller compared to the nano-strip-generated SPW. Thus, the influence of the nano-slit can be considered as a disturbance to the light distribution on the input surface. The vertical nano-slit configuration will influence the field distribution on the input surface quite differently, depending on whether the vertical nano-slit is in resonance or not[3, 9]. Our numerical simulation results have shown that both the position of the nano-slit and distance L influence significantly

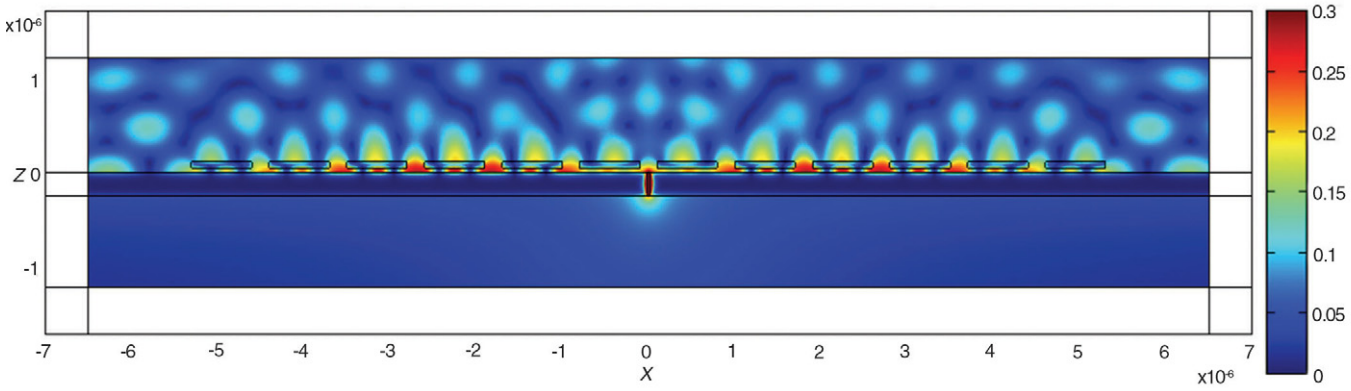

Fig. 4 Distributions of $|H_y|$ for the metallic nano-slit (Ws = 25 nm, t = 240 nm) assisted by an array of nano cavity antennas with P = 900 nm, Wp = 700 nm, L = 450 nm, Hp = 60 nm, d = 50 nm and N = 6.

the transmission of light through the nano-slit. Since non-resonant nano-slits give negligible influence to the local field distribution on the input surface, such an array of nano-cavity antennas can be combined easily with an array of non-resonant nano-slits and some potential applications can be envisaged.

Enhance transmission of low frequency TE waves through subwavelength slits in a metallic thin film by utilizing an array of electric dipole antennas

As mentioned before, many works have been carried out on enhanced transmission through subwavelength slits from optical frequencies to microwave frequencies[39-43]. However, most of them are for TM-polarized waves. Different from TM-polarized waves, transmission of a TE-polarized wave (with the electric field parallel to the slit wall) through a subwavelength slit has a cut-off frequency[86], below which no propagating modes exist. Thus, one would not expect a large transmission of low frequency TE-polarized wave (below the cut-off frequency) through subwavelength slits in a thin metallic film. Here we show how to utilize electric dipole antennas (metallic wires of finite lengths) to enhance the transmission of TE-polarized microwaves through the subwavelength slits at a resonant point below the cut-off frequency.

Fig. 5a shows the schematic diagram of a periodic array of subwavelength slits perforated in an aluminum film of thickness t. The slit width and the period of the slit array are denoted by g and p, respectively. Fig. 5b shows the cover layer composed of an array of broken metallic wires (electric dipole antennas) on a lossless dielectric layer with permittivity $\varepsilon = 3.0$ and thickness t'. The width and length of the broken wires are w and l, respectively. The period of the broken wire array in the x and y directions are p and D, respectively. Fig. 5c shows a unit cell of the combined structure when the thin cover layer is put on the top of the metal film to enhance the transmission through the subwavelength slits.

By using the three-dimensional finite-difference time-domain (FDTD) method, the transmission spectrum of the slit array (without the cover layer) with g = 5.5 mm, p = 30 mm and t = 0.5 mm is calculated and shown by the dashed (blue) curve in Fig. 6a. Since the microwave wavelength we considered here (λ > 30 mm, corresponding to frequencies below 10 GHz) is much larger than the slit width ($g < \lambda/5$), no propagating mode can be excited in these subwavelength slits for TE-polarized waves[86]. Thus the transmission can only rely on the evanescent tunneling process, and is quite low (<0.5%) even for such a thin metallic film at microwave frequencies (note that the dashed curve for the transmission is magnified by 50 times to improve the visibility in Fig. 6a). However, by adding a cover layer (the parameters for the broken wire array are l = 24 mm, w = 1.6 mm, D = 30 mm, and t' = 0.3 mm) on this array of subwavelength slits, a resonant transmission peak appears at frequency ω = 4.88 GHz (λ = 61.5 mm) with transmission up to 72% (see the blue curve in Fig. 6a), which is about 800 times larger than the transmission (at the same frequency) without the cover layer. The distribution of z-component electric field on a broken wire at the resonant frequency is shown in Fig. 6b, from which one sees charges of opposite signs accumulate at the two ends of the broken wire, indicating the excitation of a strong electric dipole resonance[87] on the broken wire. Based on the strong localized electric field near the input apertures of the slits, the incident wave is effectively coupled into evanescent waves, and then squeezed through the subwavelength slits. Consequently, a striking resonant transmission is achieved. The distribution of the corresponding electric field magnitude on the y-z plane at the edge of the broken wire is shown in Fig. 6c, from which one sees a highly localized electric field around the broken wire due to the electric dipole-like resonance. In fact, the metallic structure (shown in Fig. 6b) of the cover layer with broken wires can be regarded as a layer of metamaterial with electric resonance (which may give a negative value of the effective permittivity at a microwave frequency). Some detailed analysis will be published elsewhere.

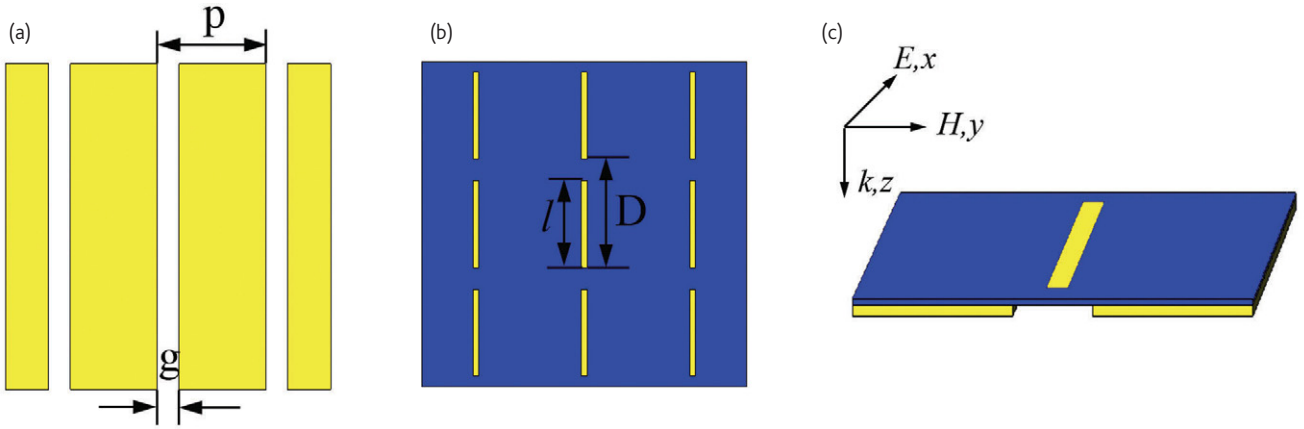

Fig. 5 Schematic diagram of (a) an aluminum film with an array of subwavelength slits; (b) a cover layer with an array of broken metallic wires; (c) unit cell for transmission calculation when the cover layer is put on the aluminum film to enhance the transmission.

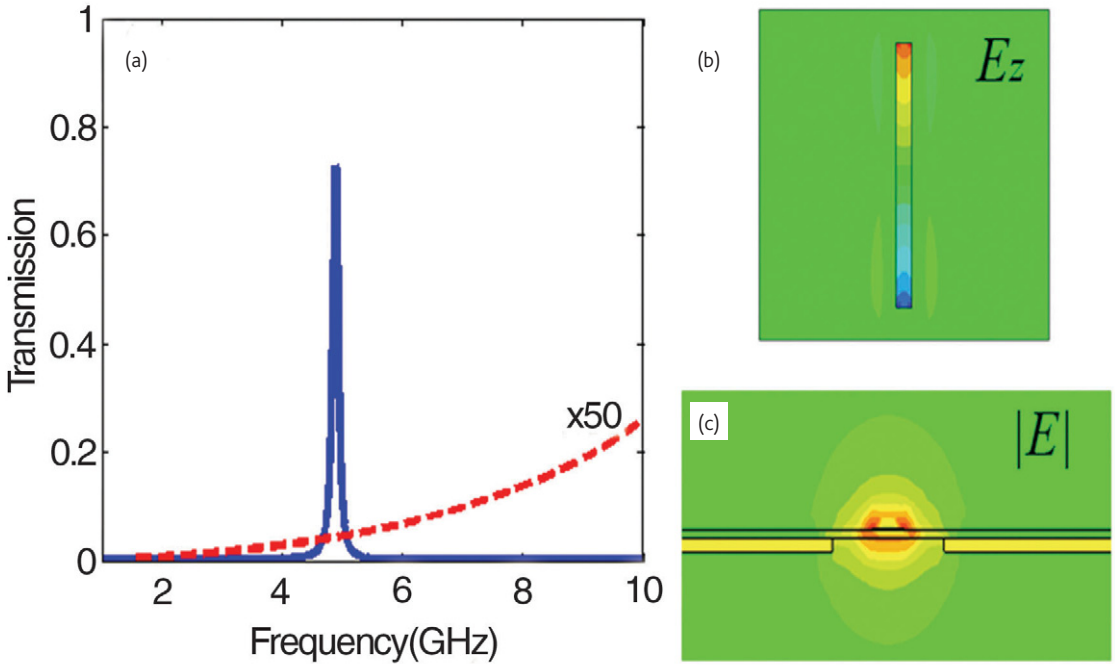

Fig. 6 (a) Transmission spectrum through the slit array without (red dashed curve) and with (blue solid curve) the cover layer. (b) Distribution of E_z on a broken wire at the resonant frequency. (c) Distribution of $|E|$ near the aperture of the subwavelength slit on the y-z plane at an edge of the broken wire.

Enhance transmission and harvest light with a horizontal slow-light photonic-crystal waveguide

As an example of enhanced transmission through an aperture in a dielectric material, we consider the resonant tunneling of a wide beam through a vertical subwavelength slow-light photonic-crystal (PC) waveguide[53]. As an important application of PCs[88-99], a slow-light PC waveguide (SPCW) can be used to enhance drastically the light-matter interactions[93-96]. In practice, efficient coupling of light into a subwavelength SPCW is an important subject[98, 99]. When a SPCW is of finite length, large reflection at the two open ports makes the waveguide behave like a F-P cavity[94]. At the resonance of a SPCW, a narrow beam can tunnel through the narrow vertical waveguide aperture efficiently. Such a resonance transmission is similar to the enhanced transmission of light through a subwavelength hole in a metal film. However, if the beam is quite wide, a large part of the beam will be directly reflected by the bulky PC (at the two horizontal side walls of the vertical SPCW) and the efficiency of the resonant tunneling is low. By utilizing an assistant horizontal SPCW, the resonant tunneling of a wide beam through the vertical SPCW can be enhanced drastically for light harvesting.

The SPCWs considered here are based on a square-lattice PC, which consists of dielectric cylinders with permittivity $\varepsilon = 12.96$ and radius $r = 0.3a$ (a is the period) in air. By removing an array of cylinders along the Γ-M direction, a vertical single-line defect waveguide is formed as shown at the bottom part of the structure in Fig. 7a.

Fig. 7b gives the dispersion curve of this waveguide. At the band edge $\omega_{edge} = 0.26277(2\pi c/a)$ (near the Γ point), the dispersion curve is rather flat so that the group velocity $v_g = \partial\omega/\partial k$ is very small and the waveguide becomes a SPCW with a very small propagation constant. Large reflection exists on the interfaces between the SPCW (of finite length) and free space, and some slow guide modes satisfying the F-P resonance condition may resonate strongly inside the waveguide. The resonant frequency of the F-P resonant mode closest to ω_{edge} is $\omega = 0.26324(2\pi c/a)$. Due to the slow propagation of light, the F-P resonant mode has a large quality factor ($Q = 2.74 \times 10^3$) (the high intensity of light here can be utilized for e.g. some nonlinear applications). In our numerical simulation, we choose a wide beam with waist width $w = 13a$. From curve 2 in Fig. 7c, one sees the transmissivity is very low (only about 0.19) although the SPCW is in resonance at $\omega = 0.26324(2\pi c/a)$.

We can use an assistant horizontal SPCW to enhance drastically the transmission of the wide beam through the above vertical SPCW. To construct a horizontal asymmetric SPCW (of finite length), we put two finite-length lines of dielectric cylinders at distance $d = a$ away from the top of the vertical SPCW as shown in Fig. 7a. The resonant frequency of the composite structure becomes $\omega = 0.26329(2\pi c/a)$, shifting a bit away from that of the individual vertical SPCW due to the interaction of the two SPCWs. The Q value is reduced to 1.90×10^3. At $\omega = 0.26329(2\pi c/a)$, a normally incident wide beam can be collected efficiently by the horizontal SPCW and then resonantly tunnels through the vertical SPCW. Curve 1 in Fig. 7c shows the drastically enhanced

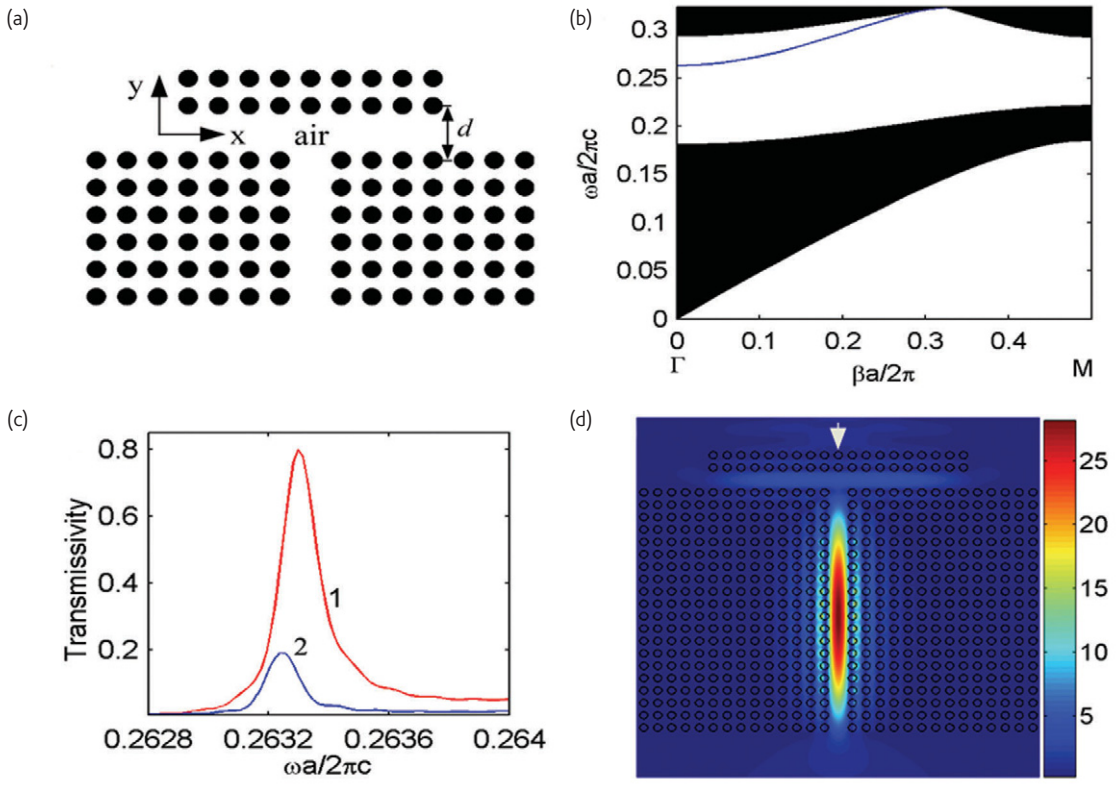

Fig. 7 (a) Harvesting light with a horizontal asymmetric SPCW (like a cavity antenna) in front of a vertical SPCW. (b) Dispersion curve of the vertical SPCW. (c) The transmissivity of a down-going wide beam (with waist w = 13a) through the vertical SPCW with (curve 1) or without (curve 2) the horizontal SPCW. The lengths of the horizontal SPCW and the vertical SPCW are 19a and 20a, respectively. (d) Distribution of $|E_z|$ at the resonant frequency of curve 1 in (b).

transmissivity when the wide beam is normally incident on the top of the structure with the assistant horizontal SPCW (like the previous resonant cavity antenna in Fig. 2a). The largest transmissivity is about 0.80 at resonant frequency $\omega = 0.26329(2\pi c/a)$. Fig. 7d shows the distribution of $|E_z|$ at $\omega = 0.26329(2\pi c/a)$. The largest $|E_z|$ is about 28 times the amplitude of the incident beam.

To harvest light more efficiently, we can use a periodic array of vertical resonant tunneling SPCWs (instead of a single SPCW) and make the horizontal SPCW infinitely long (practically several periods wider than the beam would suffice), as shown in Fig. 8a. It is found that the transmissivity becomes nearly unity when the interval between two adjacent vertical SPCWs is 9a. The periodic composite structure can act as a resonant cavity, and the resonant frequency and Q are $0.26311(2\pi c/a)$ and 2.15×10^3, respectively. Fig. 8b shows the transmissivity curve (the largest transmissivity is about 0.95). Fig. 8c shows the corresponding distribution of $|E_z|$ (the strongest $|E_z|$ inside the air gaps of the vertical symmetric SPCWs is about 33 times of the amplitude of the incident plane wave). Without the horizontal SPCW, the transmissivity will be very small (less than 0.18, see curve 2 in Fig. 8b). Obviously light has been harvested efficiently with this dielectric structure. Some details can be found in our recent work[53].

Harvest light with a metamaterial cloaking shell

A transformation-based metamaterial cloaking shell can receive incident light efficiently (even 100% when perfectly matched), and then transport the light along the shell toward the other directions. Thus, if the light is impinged on an elliptic cloaking shell (with a very large aspect ratio) from its longer side, a great amount of light could be harvested at the two far ends of the cloaking shell. In our design example, the metamaterial cloak shell has a quasi-uniform thickness (of one wavelength). The aspect ratio is 3:1 for the inner ellipse, and 2:1 for the outer ellipse. The material parameters for the cloaking shell are calculated through the standard procedure of transformation optics[73], and shown in Fig. 9a. A down-going plane wave is used as an excitation in the FEM simulation. Magnetic field distribution (magnitude) in Fig. 9b shows that the light is harvested efficiently and concentrated at the two ends of the cloaking shell. One may use only the upper half of the cloaking shell and guide the harvested light to two vertical matched strips[75].

Outlook

We have reviewed and described some approaches of optical nano-antennas and metamaterials for transmission enhancement and light

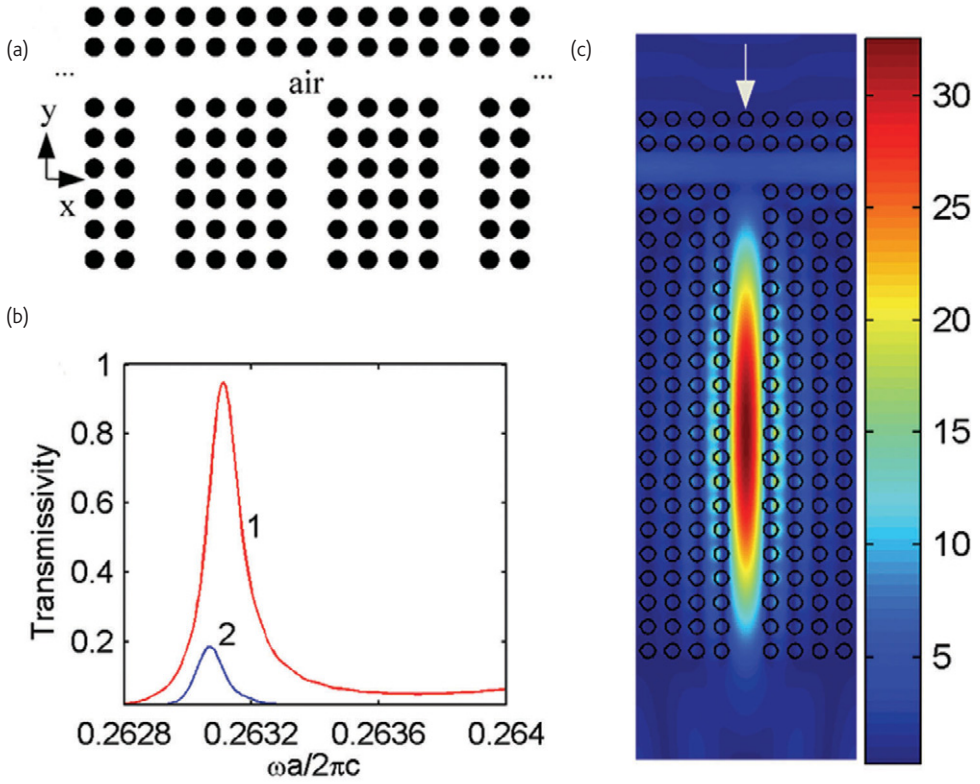

Fig. 8 (a) Harvesting light with a long horizontal asymmetric SPCW in front of a periodic array of vertical SPCWs. (b) The transmissivity of a down-going wide beam through the vertical SPCW with (curve 1) or without (curve 2) the horizontal SPCW. The length of the vertical SPCWs is 20a and the interval between two adjacent vertical SPCWs is 9a. (c) Distribution of $|E_z|$ in a unit cell at the resonant frequency of curve 1 in (b).

harvesting. Enhanced transmission of light can be utilized in many near-field optics applications, whereas light harvesting is directly related to the efficiency of solar cells. In an organic solar cell, efficient light absorption in a thin film is crucial for efficiently converting sunlight to electricity. Optical antennas can be employed to harvest external propagating light to a highly confined space for absorption in an organic solar cell. Optimally designed nano-antenna structures may improve solar cells' performances in conversion efficiency and spectral responses. We foresee that metamaterials can also play an important role in these emerging areas. mt

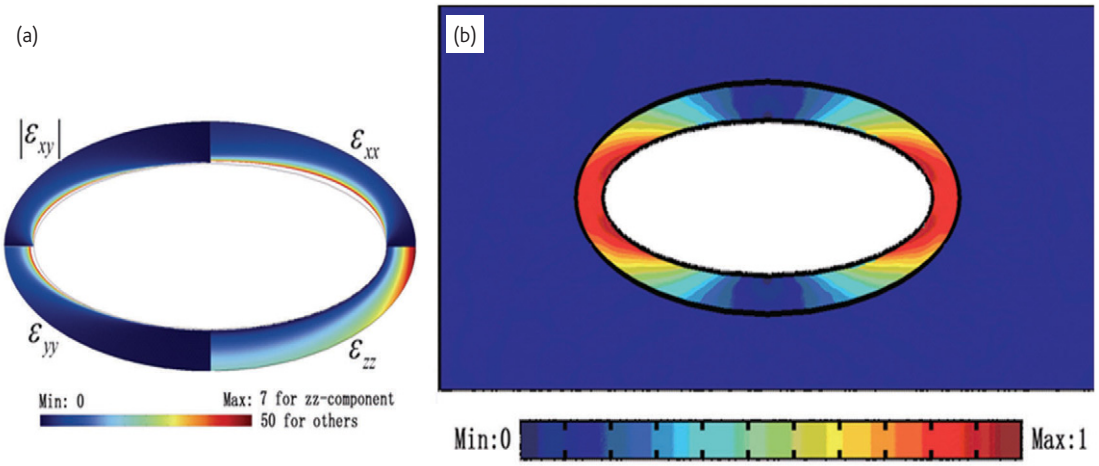

Fig. 9 (a) Non-vanishing components of the material parameters of the cloaking shell; (b) Distribution of the magnetic field magnitude (normalized) in the metamaterial cloaking shell.

Acknowledgment

This work is supported partially by the National Basic Research Program (973) of China (No. 2004CB719800), the National Science Foundation of China (90101024 and 60688401) and the Swedish Research Council (VR) under Project No. 2006-4048 and AOARD.

References

1. Ebbesen, T. W., *et al., Nature* (1998) **391**, 667.
2. Thio, T., *et al., Opt. Lett.* (2001) **26**, 1972.
3. Xie, Y., *et al., Opt. Express* (2004) **12**, 6106.
4. Takakura, Y., *Phys. Rev. Lett.* (2001) **86**, 5601.
5. Hideki, T. M., and Yoichi, K., *Phys. Rev. Lett.* (2006) **96**, 97401.
6. García-Vidal, F. J., *et al., Phys. Rev. Lett.* (2003) **90**, 213901.
7. Thio, T., *et al., Nanotechnology* (2002) **13**, 429.
8. Degiron, A., and Ebbesen, T. W., *Opt. Express* (2004) **12**, 3694.
9. Cui, Y. X., and He, S. L., *Opt. Lett.* (2009) **34**, 16.
10. Ghaemi, H. F., *et al., Phys. Rev. B* (1998) **58**, 6779.
11. Porto, J. A., *et al., Phys. Rev. Lett.* (1999) **83**, 2845.
12. Popov, E., *et al., Phys. Rev. B* (2000) **62**,16100.
13. Xie, Y., *et al., Opt. Express* (2005) **13**, 4485.
14. Gordon, R., *et al., Nano Lett.* (2005) **5**, 1243.
15. Ruan, Z. C., and Qiu, M., *Phys. Rev. Lett.* (2006) **96**, 233901.
16. Cao, Q., and Lalanne, P., *Phys. Rev. Lett.* (2002) **88**, 57403.
17. Lezec, H. J., and Thio, T., *Opt. Express* (2004) **12**, 3629.
18. Sturman, B., *et al., Phys. Rev. B* (2008) **77**, 75106.
19. Liu, H., and Lalanne, P., *Nature* (2008) **452**, 728.
20. Lezec, H. J., *et al., Science* (2002) **297**, 820.
21. Martin-Moreno, L., *et al., Phys. Rev. Lett.* (2003) **90**, 167401.
22. Yu, L. B., *et al., Phys. Rev. B* (2005) **71**, 41405.
23. Perchec, J. L., *et al., Phys. Rev. Lett.* (2006) **97**, 036405.
24. Teperik, T. V., *et al., Nat. Photon.* (2008) **2**, 299.
25. Bonod, N., *et al., Opt. Express* (2008) **16**,15431.
26. Raether, H., *Surface Plasmons*, Springer, Berlin, (1988).
27. Maier, S. A., *Plasmonics: fundamentals and applications*, Springer, New York, (2007).
28. Srituravanich, W., *et al., Nano Lett.* (2004) **4**, 1085.
29. Shao, D. B., and Chen, S. C., *Nano Lett.* (2006) **6**, 2279.
30. Levene, M. J., *et al., Science* (2003) **299**, 682.
31. Capoulade, J., *et al., Phys. Rev. Lett.* (2005) **95**, 117401.
32. Kahl, M., and Voges, E., *Phys. Rev. B* (2000) **61**, 14078.
33. Liu, C., *et al., Appl. Phys. Lett.* (2005) **86**, 143501.
34. Bahriz, M., *et al., Opt. Express* (2007), **15**, 5948.
35. Laux, E., *et al., Nat. Photon.* (2008) **2**, 161.
36. Pendry, J. B., *et al., Science* (2004) **305**, 847.
37. Miyamaru, F., *et al., Opt. Lett.* (2006) **31**, 1118.
38. Isaac, T. H., *et al., Phys. Rev. B* (2008) **77**, 113411.
39. Yang, F., and Sambles, J. R., *Phys. Rev Lett.* (2002) **89**, 63901.
40. Bravo-Abad, J., *et al., Phys. Rev. E* (2004) **69**, 26601.
41. Hibbins, A. P., *et al., Science* (2005) **308**, 670.
42. Ma, Y. G., *et al., Phys. Rev. B* (2007) **76**, 85413.
43. Lockyear, M. J., *et al., Appl. Phys. Lett.* (2007) **91**, 251106.
44. Lu, M. H., *et al., Phys. Rev. Lett.* (2007) **99**, 174301.
45. Akimov, A. V., *et al., Phys. Rev. Lett.* (2008) **101**, 33902.
46. Fernandez-Dominguez, A. I., *et al., Phys. Rev. A* (2008) **78**, 23614.
47. Kuhn, S., *et al., Phys. Rev. Lett.* (2006) **97**, 17402.
48. Schuck, P. J., *et al., Phys. Rev. Lett.* (2005) **94**, 17402.
49. Muhlschlegel, P., *et al., Science* (2005) **308**, 1607.
50. Tang, L., *Nat. Photon.* (2008) **2**, 226.
51. Merlein, J., *et al., Nat. Photon.* (2008) **2**, 230.
52. Taminiau, T. H., *et al., Nat. Photon.* (2008) **2**, 234.
53. Jin, Y., and He, S. L., *Opt. Express.* (2008) **16**, 19550.
54. Wood, B., *Laser Photon. Rev.* (2007) **1**, 249.
55. Yu, K., *et al., Rev. Mod. Phys.* (2008) **80**, 1201.
56. Soukoulis, C. M., *et al., J. Phys.: Condens. Matter.* (2008) **20**, 304217.
57. Veselago, V. G., *Sov. Phys. Usp.* (1968) **10**, 509.
58. Pendry, J. B., *et al., IEEE Trans. Micr. Theory & Tech.* (1999) **47**, 2075.
59. Shelby, R. A., *et al., Science* (2001) **292**, 77.
60. Linden, S., *et al., Science* (2004) **306**, 5700.
61. Shalaev, V. M., *et al., Opt. Lett.* (2005) **30**, 3356.
62. Pendry, J. B., *Phys. Rev. Lett.* (2000) **85**, 3966.
63. Fang, N., *et al., Science* (2005) **308**, 534.
64. Chen, L., *et al., Phys. Rev. Lett.* (2004) **92**,107404.
65. He, S. L., *et al., New J. Phys.* (2005) **7**, 210.
66. Liu, L., and He, S. L., *Opt. Express* (2004) **12**, 4835.
67. Sihvola, A., *et al., J. Comm. Tech. & Electron.* (2007) **52**, 986.
68. Alu, A., *et al., IEEE Antenn. & Propag. Mag.* (2007) **49**, 23.
69. Silveirinha, M., and Engheta, N., *Phys. Rev. Lett.* (2006) **97**, 157403.
70. Landy, N. I., *et al., Phys. Rev. Lett.* (2008) **100**, 207402.
71. He, J. L., and He, S. L., *IEEE Microw. & Wireless Compon. Lett.* (2006) **16**, 96.
72. Hao, J. M., *et al., Phys. Rev. Lett.* (2007) **99**, 63908.
73. Pendry, J. B., *et al., Science* (2006) **312**, 1780.
74. Chen, H., *et al., Phys. Rev. Lett.* (2007) **99**, 63903.
75. Cummer, S. A., *et al., Phys. Rev. E* (2006) **99**, 36621.
76. Schurig, D., *et al., Science* (2006) **314**, 977.
77. Liu, R., *et al., Science* (2009) **323**, 366.
78. Yan, M., *et al., Opt. Express* (2007)**15**, 17772.
79. Jiang, W. X., *et al., Phys. Rev. E.* (2008) **77**, 66607.
80. Zhang, P., *et al., Appl. Phys. Lett.* (2008) **93**, 243502.
81. Cummer, S. A., and Schurig, D., *Phys. Rev. Lett.* (2008) **100**, 24301.
82. Zhang, S., *et al., Phys. Rev. Lett.* (2008) **100**, 123002.
83. Pillai, S., *et al., J. App. Phys.* (2007) **101**, 93105.
84. Li, X., *et al., Nanotechnology* (2008) **19**, 355501.
85. Li, X., *et al., Appl. Phys. Lett.* (2009) **94**, 063111.
86. Kong, J. A., *Electromagnetic Wave Theory*, John Wiley and Sons, New York, (1986).
87. Zhou, J., *et al., Opt. Express* (2007) **15**, 17881.
88. Sakoda, K., *Optical Properties of Photonic Crystals*, Springer, Berlin, (2001).
89. Krauss, T. F., *J. Phys. D: Appl. Phys.* (2007) **40**, 2666.
90. Baba, T., *Nat. Photon.* (2008) **2**, 465.
91. Mori, D., and Baba, T., *Appl. Phys. Lett.* (2004) **85**, 1101.
92. Petrov, A. Y., and Eich, M., *Appl. Phys. Lett.* (2004) **85**, 4866.
93. Soljačić, M., *et al., J. Opt. Soc. Am. B* (2002) **19**, 2052.
94. Kiyota, K., *et al., Appl. Phys. Lett.* (2006) **88**, 201904.
95. Beggs, D. M., *et al., Opt. Lett.* (2008) **33**, 147.
96. He, J. L., *et al., Opt. Express* (2008) **16**, 11077.
97. Vlasov, Y. A., *et al., Nature* (2005) **438**, 65.
98. Vlasov, Y. A., and McNab, S. J., *Opt. Lett.* (2006) **31**, 50.
99. Hugonin, J. P., *et al., Opt. Lett.* (2007) **32**, 2638.